

# Phase step calibration and phase measurement in image plane holography using BaTiO<sub>3</sub> crystal as a recording medium

**S. Suja Helen**

**M. H. Majles Ara**, MEMBER SPIE

**J. S. Darlin**

Indian Institute of Technology  
Department of Physics  
Applied Optics Laboratory  
Madras 600 036, India

**N. Krishna Mohan**

National Research Council  
Institute for National Measurement  
Standards  
Optics Group  
Ottawa, Ontario K1A 0R6  
Canada

**M. P. Kothiyal**

Indian Institute of Technology  
Department of Physics  
Applied Optics Laboratory  
Madras 600 036, India

**R. S. Sirohi**, FELLOW SPIE

National University of Singapore  
Department of Mechanical and Production  
Engineering  
Singapore

## 1 Introduction

Holographic interferometry and speckle photography were successfully demonstrated with a BSO crystal by Huignard et al.<sup>1</sup> and Tiziani et al.,<sup>2</sup> respectively. Since then, photorefractive materials such as BSO, BGO, BTO, SBN, BaTiO<sub>3</sub>, LiNbO<sub>3</sub>, etc. have found potential use in image processing, speckle photography, and holographic interferometry<sup>3-13</sup> (HI). The attractive features of the photorefractive crystals are high resolution, real-time processing, and no development. Double-exposure as well as time-average recordings were performed with photorefractive crystals as recording media for static deformation measurements and vibration analysis.<sup>14-16</sup> The real-time measurements were demonstrated with either two-wave-mixing or four-wave-mixing configurations. The applications of photorefractive crystals such as BaTiO<sub>3</sub>, LiNbO<sub>3</sub>, etc. are characterized by slow response times, requiring longer exposures than fast-response crystals such as BSO.

Recently we used BaTiO<sub>3</sub> crystals as a recording medium extensively as a novelty filter for real-time measurements because of its slow response time. A two-beam coupling configuration was implemented for crystal parameter characterization and optimization studies.<sup>17</sup> These studies include measurement of diffraction efficiency, grating formation and erase rates. We also emphasized that the slow

**Abstract.** A real-time visual approach for the calibration of phase step in image plane holography using BaTiO<sub>3</sub> crystal as a recording medium is reported. In this method, the diffuse object is illuminated symmetrically with two collimated beams and a pump beam is added at the crystal plane. Each illuminating beam generates an individual interferogram at the observation plane when the object is subjected to load. A  $\pi$  phase shift to one of the illuminating beams results in the complete disappearance of the fringes due to phase reversal between the individual interferograms, and at  $2\pi$  phase change, the fringe pattern is restored. After calibration, a single-beam illumination configuration is used for phase measurement. We present the theory of the method and experimental results for a centrally loaded diaphragm rigidly clamped along the periphery. © 1998 Society of Photo-Optical Instrumentation Engineers. [S0091-3286(98)01611-0]

Subject terms: photorefractive effect; phase measurement; two-beam coupling; interferometry; holography; image processing.

Paper 980024 received Jan. 21, 1998; revised manuscript received July 6, 1998; accepted for publication July 17, 1998.

response time of the BaTiO<sub>3</sub> crystal can be used to our advantage to perform dynamic holography by skillful management of exposure times. The slow response takes a finite time ( $\sim 10$  s for typical experimental conditions) to reach its steady state, and the dynamic grating (corresponding to the initial state of the object) created inside the crystal takes fairly long time to decay ( $\sim 100$  s under typical experimental conditions). We showed that within this decay time it is possible to sequentially compare various deformation states of the object. Recently we carried out two types of dynamic studies exploiting the slow response time of the BaTiO<sub>3</sub> crystal; when (1) the object state is continuously changing with time and (2) the change in object state is discrete.<sup>17</sup>

In the first method, the initial state of the object is recorded in the crystal by allowing the object and the pump beams to interfere inside the crystal. Once the two-beam coupling reaches its steady state, the object is deformed. The change in the object due to deformation disturbs the two-beam coupling process. Due to the continuous change in the object, and hence in the object beam, after this instant of time, two-beam coupling is never established. Then at the observation plane we observe the interference between the diffracted pump beam and continuously changing directly transmitted object beam. The fringe pattern at the

observation plane also constantly changes due to the sequential comparison of the present state of the object with its initial state. This is a situation similar to that in real-time HI. The dynamic events pertaining to object deformation can be monitored by continuously grabbing the frames. This enables us to grab several frames over the grating decay period. However, the changes in the object should take place within a time that is much shorter than the time required for two-beam coupling to become established between the new object beam and the pump beam.

In the second method, where the object changes take place in discrete steps, with the time delay between the consecutive steps being much longer than that required to establish two-beam coupling, it becomes necessary to block the writing beams at each step. In this method, after the initial grating has reached its steady state, the writing beams (both the object and pump beams) are cut off, and after each loading of the object, the writing beams are allowed to fall on the crystal for a period that is much shorter than that required to establish two-beam coupling. The process is continued in steps, with the beams being cut off after each exposure. The continuous step method is used for phase step calibration, while the discrete step method is employed in this paper for phase measurement.

Phase-shift interferometry is well established and implemented in interferometry, HI (Ref. 18), and electronic speckle pattern interferometry for quantitative analysis of the deformation of an object.<sup>19</sup> The phase-shifting technique for quantitative evaluation of an interferogram using attractive media such as photorefractive crystals has gained considerable interest in the recent years. Dirksen and von Bally<sup>20</sup> combined a double-exposure BTO interferometer with a Fourier-transform-based analysis method for deformation analysis. Georges and Lemaire<sup>21</sup> recently implemented phase-shifting techniques in a BSO interferometer. It is well known that the major source of error in the phase-shifting technique is phase-shift miscalibration error.<sup>22-24</sup> Therefore phase step calibration is an important factor in obtaining an error-free phase map. The aim of this paper is to implement the phase-shifting technique in image plane holography using a BaTiO<sub>3</sub> crystal as a recording medium. A real-time visual method employing a dual-beam illumination configuration for phase step calibration is presented in Sec. 2. In this method, the unshifted interferogram generated from one of the illumination beams is compared with the phase-shifted interferogram obtained from the other illumination beam. The calibrated phase steps are incorporated by adopting the four-phase-step method for phase measurement. Section 3 describes the method and shows the experimental results obtained from a diaphragm rigidly clamped along the periphery and loaded at the center.

## 2 Phase Step Calibration with a Dual-Beam Illumination Configuration

### 2.1 Experimental Arrangement

Figure 1 shows a schematic of the experimental setup. It basically consists of a standard image plane holography system. The beam from a 35-mW He-Ne laser is divided by a variable beamsplitter (VBS). The object beam is again split into two beams *A* and *B* of equal amplitudes via a beamsplitter (BS) and filtered through the spatial filters SF<sub>1</sub>

and SF<sub>2</sub> and then collimated by lenses *L*<sub>1</sub> and *L*<sub>2</sub>. Both beams illuminate the object symmetrically at angles  $\theta$  and  $-\theta$  with respect to object normal via mirror *M* and another mirror driven by a piezoelectric translator (PZTM). The object is imaged onto a BaTiO<sub>3</sub> crystal ( $5 \times 5 \times 5$  mm) by lens *L*<sub>3</sub> and an expanded 5-mm-diam pump beam is added at the crystal, making an angle  $2\Omega$  with respect to the object beam. An additional imaging lens *L*<sub>4</sub> images the object onto the surface of the CCD camera. The CCD camera is connected to a commercially available image processing system that is interfaced to the host computer for image grabbing and processing. The *c* axis of the crystal is oriented in such a way that the spatial phase shift  $\varphi$  between the incident interference pattern and the resulting index grating is  $\pi/2$  so that the object beam becomes amplified due to the diffraction of the pump beam in the direction of the object beam.<sup>15</sup> The field diffracted from the grating represents the initial state of the object at the image plane of lens *L*<sub>4</sub>.

### 2.2 Fringe Formation Analysis

In the present configuration, two gratings are formed during the initial stage due to the interference of each of the illuminating beams with the pump beam. After allowing sufficient time for the two-beam coupling process to reach steady state, a constant voltage is applied to the PZTM, thereby introducing an arbitrary phase step  $\alpha$  to illuminating beam *A*. In addition, the object is also deformed. Phase step  $\alpha$  and the object deformation introduce a phase variation in the object beams and consequently in the image field distribution inside the crystal. At this instant, at the CCD (observation) plane, we have four beams—two beams, which constitute the initial state of the object, are due to diffraction of the pump beam from the gratings formed at the initial stage, and the other two beams are the directly transmitted object beams, which constitute the present state of the object with unknown phase step and deformation of the object. In other words, two waves generated from the decaying grating and two waves directly transmitted interact at the image plane and the amplitudes of four interacting beams at some instant of time *t* are given as

$$a_1(t) = a_{01}(t) \exp[i(\phi_1)], \quad (1)$$

$$a_2(t) = a_{02}(t) \exp[i(\phi_2)], \quad (2)$$

$$a_3(t) = a_{03}(t) \exp[i(\phi_1 + \delta_1 + \alpha)], \quad (3)$$

$$a_4(t) = a_{04}(t) \exp[i(\phi_2 + \delta_2)], \quad (4)$$

where  $\phi_1$  and  $\phi_2$  are the random phases of the object beam generated by two illumination beams, and  $\delta_1$  and  $\delta_2$  are phase changes due to the object deformation.

Because the amplitudes of the four interacting beams are a function of time *t*, at some time instant when the amplitudes of the four beams are equal, the intensity distribution in the interference pattern at the image plane is given by<sup>17</sup>

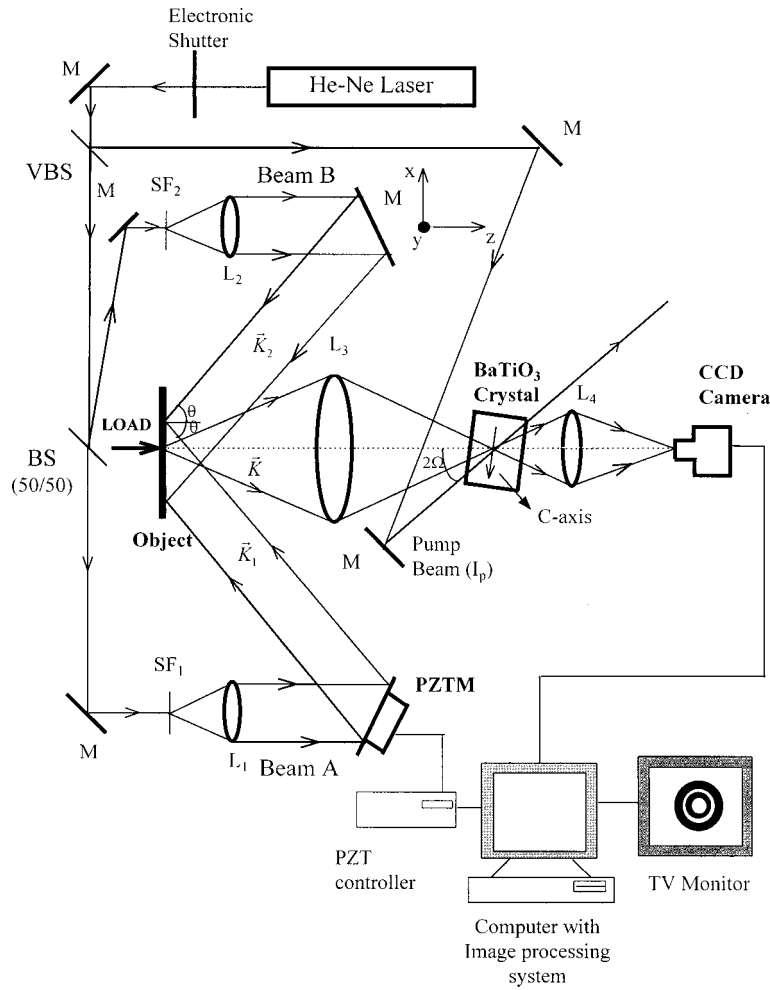


Fig. 1 Schematic of a dual-beam illumination configuration for phase step calibration.

$$\begin{aligned}
 I = I_0 [ & 4 + 2 \cos(\phi_{21}) + 2 \cos(\phi_{21} - \delta_1 - \alpha) \\
 & + 2 \cos(\phi_{21} + \delta_2) + 2 \cos(\phi_{21} + \delta_2 - \delta_1 - \alpha) \\
 & + 2 \cos(\delta_1 + \alpha) + 2 \cos(\delta_2) ], \quad (5)
 \end{aligned}$$

where  $\phi_{21} (= \phi_2 - \phi_1)$  is the random phase.

It can be seen from Eq. (5) that the terms containing  $\phi_{21}$  generate the speckle image and only the last two terms contribute to the fringe formation. Two individual interferograms result from this configuration, one due to illumination, the observation vector pair  $(\mathbf{k}_1, \mathbf{k})$ , and the other due to the illumination, the observation vector pair  $(\mathbf{k}_2, \mathbf{k})$ . The phase changes  $\delta_1$  and  $\delta_2$  due to object deformation can be written as

$$\begin{aligned}
 \delta_1 &= (\mathbf{k} - \mathbf{k}_1) \cdot \mathbf{L}, \\
 \delta_2 &= (\mathbf{k} - \mathbf{k}_2) \cdot \mathbf{L}, \quad (6)
 \end{aligned}$$

where  $\mathbf{L}(u, v, w)$  is the deformation vector at a point on the object surface and  $u, v,$  and  $w$  are its components, i.e.,  $\mathbf{L} = u\hat{i} + v\hat{j} + w\hat{k}$  ( $\hat{i}, \hat{j},$  and  $\hat{k}$  are unit vectors along the  $x, y,$  and  $z$  directions).

The phase changes carry the information pertaining to in-plane displacement components as well as out-of-plane displacement. Assuming that the illuminating beams lie in the  $x-z$  plane, we can express the phase changes  $\delta_1$  and  $\delta_2$  as<sup>18</sup>

$$\delta_1 = \frac{2\pi}{\lambda} [u \sin \theta + w(1 + \cos \theta)], \quad (7)$$

$$\delta_2 = \frac{2\pi}{\lambda} [-u \sin \theta + w(1 + \cos \theta)]. \quad (8)$$

Equation (7) represents a fringe pattern due to in-plane displacement component  $u$  plus the out-of-plane displacement  $w$ , while Eq. (8) gives the fringe patterns due to minus in-plane displacement component  $u$  plus out-of-plane displacement  $w$ . In addition, an unknown phase step  $\alpha$  to the illuminating beam A introduces an additional phase shift to the fringe pattern obtained from Eq. (7). The resultant fringe pattern due to both illuminating beams A and B is a moiré pattern. This moiré pattern has a very low contrast, hence is of a little practical use for phase step calibration. On the other hand, if the object is subjected to only either

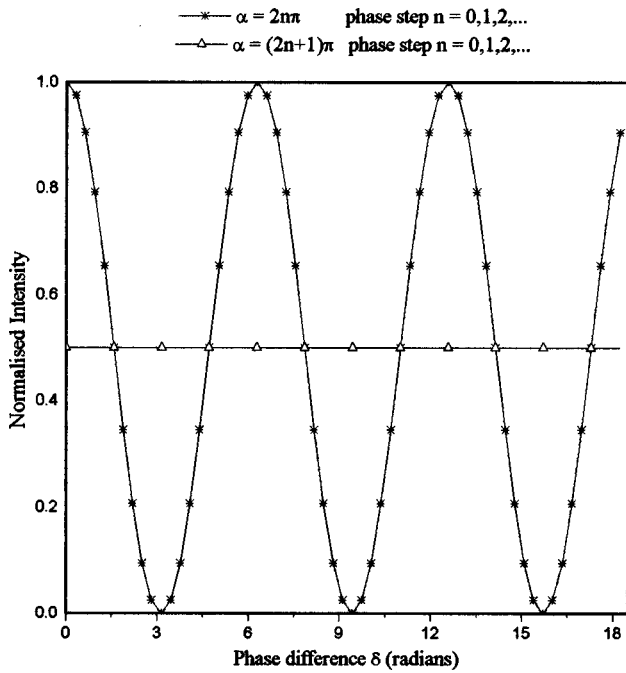


Fig. 2 Irradiance distribution profile with two-beam illumination configuration.

in-plane displacement ( $u \gg w$ ) or out-of-plane displacement ( $w \gg u$ ), then the fringe patterns generated by individual beams can be adopted for visual phase step calibration. If the illumination beams illuminate the object normally, this requirement is not necessary.

**2.2.1 Case 1: Phase step  $\alpha = 0$**

In the optical arrangement, when there is no phase stepping, Eq. (5) for the intensity distribution due to interaction of four beams at the image plane reduces to

$$I = I_0 [4 + 2 \cos(\phi_{21}) + 2 \cos(\phi_{21} - \delta_1) + 2 \cos(\phi_{21} + \delta_2) + 2 \cos(\phi_{21} + \delta_2 - \delta_1) + 2 \cos(\delta_1) + 2 \cos(\delta_2)]. \tag{9}$$

If the object is subjected to a small out-of-plane displacement  $w$ , then the fringe patterns generated by individual beams  $A$  and  $B$  are identical, and the combined pattern is also the same. Phase changes  $\delta_1$  and  $\delta_2$  can be related to the out-of-plane displacement  $w$  as

$$\delta_1 = \delta_2 = \delta = \frac{2\pi}{\lambda} (1 + \cos \theta) w = 2m\pi. \tag{10}$$

When this condition is satisfied, the intensity distribution in the interference pattern is given by

$$I = 4I_0(1 + \cos \phi_{21})(1 + \cos \delta). \tag{11}$$

Taking all these parameters into consideration, the normalized overlapped irradiance generated by individual illumination beams  $A$  and  $B$  with pump beam is shown in Fig. 2. While plotting the intensity distribution, we have not

taken into account the associated random speckle phase terms  $\phi_{21}$  in the Eq. (11), which contribute additional back-group noise to the interferograms.

**2.2.2 Case 2: Phase step  $\alpha = \pi$**

When the phase step is exactly equal to  $\pi$ , the intensity distribution in Eq. (5) reduces to

$$I = I_0 [4 + 2 \cos(\phi_{21}) + 2 \cos(\phi_{21} - \delta_1) + 2 \cos(\phi_{21} + \delta_2) + 2 \cos(\phi_{21} + \delta_2 - \delta_1) - 2 \cos(\delta_1) + 2 \cos(\delta_2)]. \tag{12}$$

The individual patterns generated due to phase terms  $\delta_1$  and  $\delta_2$  are phase (contrast) reversed with respect to each other. This results in a fringe-free field on the monitor with a constant bias ( $I = 4I_0$ ) for the case when  $\delta_1 = \delta_2 = \delta$ . This intensity distribution, which represents as a constant irradiance distribution, is also plotted and shown in Fig. 2. It is evident from the graph that the fringes disappear completely when the phase shift is exactly  $\pi$ , and this condition repeats whenever the phase shift  $\alpha$  is  $(2n+1)\pi$ ,  $n = 0, 1, 2, 3, \dots$

**2.2.3 Case 3: Phase step  $\alpha = 2\pi$**

When the phase step  $\alpha = 2\pi$ , the intensity distribution equation is the same as given by Eq. (11), and also the interferograms obtained are identical, as defined in Eq. (10). The phase-shifted fringe pattern generated from illuminating beam  $A$  with reference to the unshifted fringe pattern obtained from illuminating beam  $B$  is same for even multiples of  $\pi$  (the phase step  $\alpha = 2n\pi$ ).

**2.3 Experimental Results**

The experimental calibration is carried out on a centrally loaded diaphragm rigidly clamped along the periphery and loaded at the center to produce an out-of-plane deflection. The specimen is illuminated symmetrically at angles  $20$  and  $-20$  deg with two collimated beams of  $30$  mm diameter. The expanded pump beam of higher intensity is added at the crystal at an angle of  $20$  deg with respect to the object beam. The polarizations of all the beams are chosen in such a way that they are  $e$  polarized inside the crystal to exploit the maximum electro-optic coefficient  $\gamma_{42}$  (Ref. 17). For phase step calibration and measurement, a low-voltage PZT driver with a position sensor (Model PI 810, Physik Instruments, Germany) is used in the setup. Initially the PZT mirror is not activated (the phase step  $\alpha = 0$ ). Due to the slow response time of the  $\text{BaTiO}_3$  crystal, the amplification of the object beam takes a finite time ( $\sim 10$  s) to reach steady state. Once the hologram formation reaches its steady state, the object is given a small out-of-plane deflection, resulting in an appearance of fringes instantaneously. The real-time fringe patterns recorded directly from the TV monitor with one illuminating beam at a time are shown in Figs. 3(a) and 3(b). When both illuminating beams are used simultaneously, the resultant fringe pattern is also the same as obtained with individual beams since the object deformation is practically out of plane. The combined pattern is shown in Fig. 3(c). Now the PZT mirror is activated and

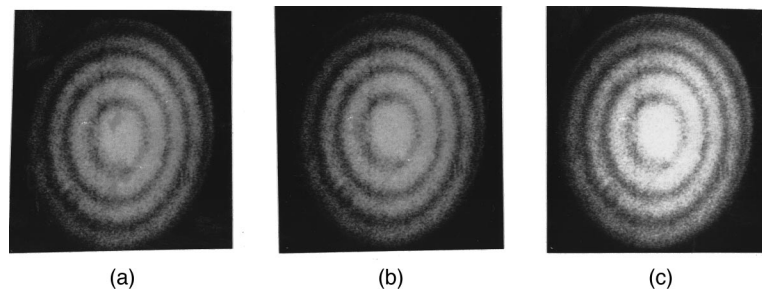


**Fig. 3** Fringe patterns obtained with the two-beam illumination configuration when the phase step  $\alpha = 0$ : (a) and (b) fringes recorded with one-at-a-time individual illumination beams and (c) fringes obtained when both illuminating beams are simultaneously present. The fringe patterns are identical in the present situation, and they are the same for even multiples of  $\pi$  phase shift.

the voltage is applied in a controlled manner using a PZT controller via the host computer. The phase-shifted fringe patterns are observed continuously on the monitor with reference to the unshifted fringe pattern generated from the other illuminating beam. The combined fringe pattern is also monitored during the calibration for different applied voltages. At a particular applied voltage, the combined fringe pattern completely disappears on the monitor and this voltage corresponds to a phase shift  $\pi$ .

The stored interferograms when the phase shift  $\alpha = \pi$  are shown in Figs. 4(a) and 4(b) with one illumination beam each and in Fig. 4(c) when both beams illuminate the object. The simulated fringe patterns based on the theoretical solutions and experimental parameters when the phase shift exactly equals  $\pi$  are shown in Figs. 5(a) and 5(b) for the case of one illumination beam and for the case of both illumination beams, respectively. Figure 6 shows the visual calibration achieved by observing the fringe patterns on the monitor extended up to  $14\pi$  phase shift and the phase shift as a function of applied voltage. In the present setup, only small voltages are required to drive the PZT for the required phase steps, and the phase step is linear with the applied voltage. The repeatability in phase step calibration is carried out a number of times by varying the input voltage from zero to maximum. From the experimental results for a 54-mV input signal which provides a phase shift of  $\pi$ , the accuracy of the phase step measured is around 0.17 deg.

### 3 Phase Measurement

The optical arrangement is same as shown in Fig. 1 except that illumination beam  $B$  is blocked for phase measurement. Once the two-beam coupling process reaches its steady state, the object is subjected to a small out-of-plane displacement. This disturbs the two-beam coupling process and results in an interferogram due to the interference of the diffracted pump beam and directly transmitted object beam at the CCD plane. The interferogram due to object deformation is stored in the host computer. The interferograms with calibrated phase steps achieved by shifting the PZT mirror in the object beam are also stored in the computer. To store the shifted fringe patterns, a discrete step method,<sup>17</sup> as mentioned earlier, in which the writing beams are blocked at each phase step is used here. In this, once the initial interferogram, which represents the deformation of an object, is stored, the writing beams (both object and pump beams) are cut off by closing the electronic shutter in front of the laser beam. During each phase step change, the writing beams are allowed to fall on the crystal, with an exposure time much smaller than that required for establishing two-beam coupling. The process is continued in steps, with the beams being cut off after each phase step. In each step, at the observation plane, the initial state of the object is compared with the phase shifted deformed state

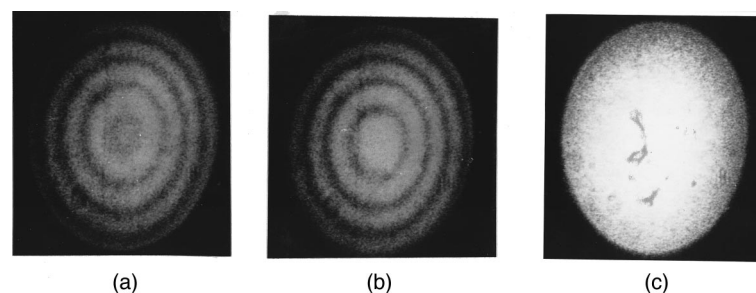


**Fig. 4** Interferograms obtained with the two-beam illumination method: (a)  $\pi$  phase-shifted fringe pattern obtained from illumination beam  $A$  when illuminating beam  $B$  is blocked, (b) unshifted fringe patterns from illumination beam  $B$  when illuminating beam  $A$  is blocked, and (c) fringe-free field with a constant bias when both illuminating beams are simultaneously present.

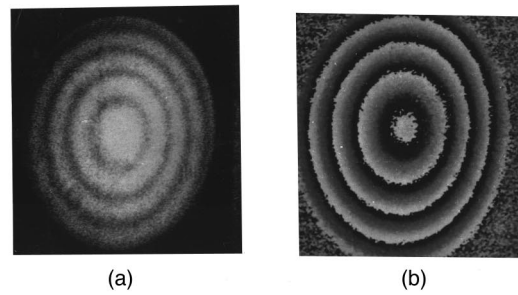
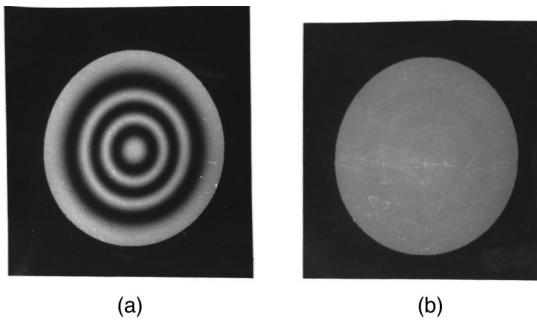


**Fig. 5** Simulated fringe patterns based on the theoretical solutions and experimental parameters generated for  $\pi$  phase shift. These fringe patterns are same as shown in Figs. 4(b) and 4(c).

and the resulting interferograms are grabbed. The irradiance distribution in each interferogram at any pixel on the detector array can be expressed as

$$I = I_0 [1 + V \cos(\delta + \alpha)], \tag{13}$$

where  $\alpha$  is the phase step,  $V$  is the modulation factor, and  $\delta$  is the phase to be measured. The phase change  $\delta$  is calculated pixel by pixel with the help of the following four-step algorithm

$$\delta = \tan^{-1} \left( \frac{I_4 - I_2}{I_1 - I_3} \right), \tag{14}$$

where  $I_1, I_2, I_3,$  and  $I_4$  are the intensities corresponding to the phase shifts  $\alpha = 0, \pi/2, \pi,$  and  $3\pi/2,$  respectively. The result is the module  $2\pi$  phase map of the original interferogram.

The relationship between the wavefront phase and the surface deformation  $w$  is given by<sup>18</sup>

$$w = \frac{\lambda \delta}{2\pi(1 + \cos \theta)}. \tag{15}$$

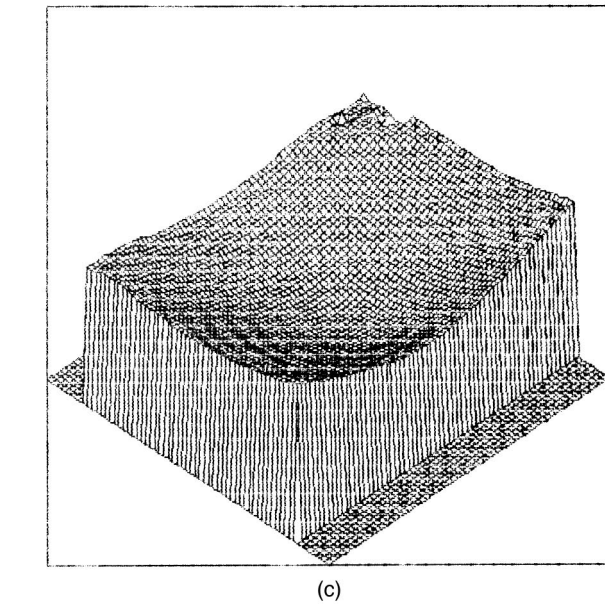


**Fig. 7** Results obtained with the single-beam illumination image plane holography configuration: (a) the fringe pattern photographed directly from the monitor, (b) the raw phase map, and (c) the 3-D plot of the surface deformation from the phase maps after the removal of  $2\pi$  phase ambiguity.

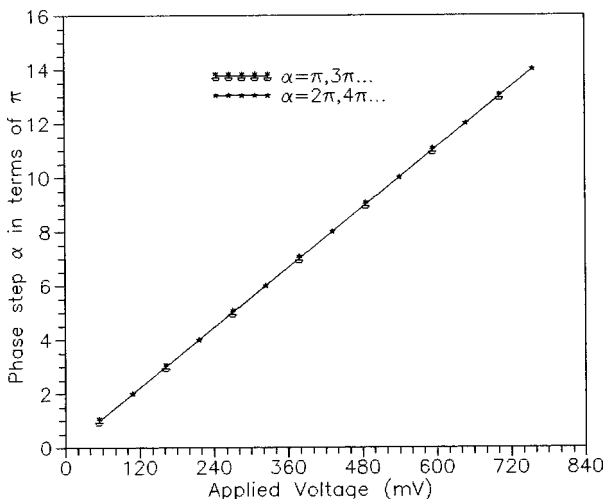


**Fig. 6** Linear relationship of the phase step with the applied voltage obtained from the real-time visual observation configuration.

The experimental results for a centrally loaded diaphragm rigidly clamped along the periphery are shown in Fig. 7. Figure 7(a) shows the out-of-plane displacement fringes and the pattern is low-pass filtered using a  $3 \times 3$  convolution window, and the raw phase map is shown in Fig. 7(b). The  $2\pi$  phase ambiguity in the raw phase plot is corrected and scaled by Eq. (15) to obtain the 3-D plot depicting surface deformation of an object. Figure 7(c) represents the out-of-plane distribution  $w$  generated from the corrected phase map.

#### 4 Conclusion

We presented a simple real-time visual method for phase step calibration and phase measurement using a novelty whole-field filtering technique with a  $\text{BaTiO}_3$  crystal as a recording medium. The phase step is introduced by changing the phase of the illumination beam. The phase-shifting technique can be implemented by shifting the phase of the pump beam also. It is also demonstrated that

the slow response time of the BaTiO<sub>3</sub> crystal can be used for phase measurement by skillful management of exposure times.

### Acknowledgments

This work is supported by research grants from Department of Science and Technology Project on photorefractive materials for real-time holography and Department of Atomic Energy project on optical instrumentation.

### References

1. J. P. Huignard, J. P. Herriau, and T. Valentin, "Time average holographic interferometry with photoconductive electro-optic Bi<sub>12</sub>SiO<sub>20</sub> crystals," *Appl. Opt.* **16**, 2796–2800 (1977).
2. H. J. Tiziani, K. Leonhardt, and J. Klenk, "Real-time displacement and tilt analysis by a speckle technique using Bi<sub>12</sub>SiO<sub>20</sub> crystal," *Opt. Commun.* **34**, 327–331 (1980).
3. Y. H. Ja, "Real-time image division in four-wave mixing with photorefractive BGO crystal," *Opt. Commun.* **44**, 24–28 (1982).
4. S. Collicot and L. Hesselink, "Real-time photorefractive recording and optical processing for speckle velocimetry," *Opt. Lett.* **13**, 348–350 (1988).
5. K. Nakagawa and T. Minemoto, "Readout properties of the specklegram recorded in photorefractive Bi<sub>12</sub>SiO<sub>20</sub> crystal," *Appl. Opt.* **30**, 2386–2392 (1991).
6. L. Liu, H. Helmers, and K. Hinsch, "Speckle metrology with novelty filtering using photorefractive two-beam coupling in BaTiO<sub>3</sub> crystal," *Opt. Commun.* **100**, 19–23 (1993).
7. P. R. Sreedhar, N. Krishnamohan, and R. S. Sirohi, "Real-time photography with two wave mixing in photorefractive BaTiO<sub>3</sub> crystal," *Opt. Eng.* **33**, 1989–1995 (1994).
8. J. P. Huignard and P. Gunter, Eds., *Photorefractive Materials and Their Applications II*, Springer-Verlag, Berlin (1988).
9. M. P. Petrov, S. I. Stepanov, and A. V. Khomenko, *Photorefractive Crystals in Coherent Optical Systems*, Springer-Verlag, Berlin (1991).
10. R. C. Troth and J. C. Dainty, "Holographic interferometry using anisotropic self-diffraction in Bi<sub>12</sub>SiO<sub>20</sub>," *Opt. Lett.* **16**, 53–55 (1991).
11. S. L. Sochava, R. C. Troth, and S. I. Stepanov, "Holographic interferometry using 1-order diffraction in Bi<sub>12</sub>SiO<sub>20</sub> and Bi<sub>12</sub>TiO<sub>20</sub> crystals," *J. Opt. Soc. Am. B* **9**, 1521–1527 (1992).
12. J. Joseph, K. Kamra, K. Singh, and P. K. C. Pillai, "Real-time image processing using selective erasure in photorefractive two-wave mixing," *Appl. Opt.* **31**, 1–5 (1992).
13. A. Shiratori and M. Obara, "High-resolution surface sensing device using Bragg diffraction from multiplexed holograms in photorefractive crystal," *Rev. Sci. Instrum.* **67**, 3017–3020 (1996).
14. J. P. Herriau, A. Delboulbe, and J. P. Huignard, "Nondestructive testing using real time holographic interferometry in BSO crystal," *Proc. SPIE* **398**, 123–126 (1983).
15. P. R. Sreedhar, N. Krishnamohan, and R. S. Sirohi, "Deformation studies with BaTiO<sub>3</sub> crystal as recording medium," *Proc. SPIE* **2340**, 40–43 (1994).
16. B. Pouet and S. Krishnaswamy, "Dynamic holographic interferometry by photorefractive crystals for quantitative deformation measurements," *Appl. Opt.* **35**, 787–794 (1996).
17. P. R. Sreedhar, "Real time image processing and hologram Interferometry with BaTiO<sub>3</sub> crystal," Ph.D Thesis, Indian Institute of Technology, Madras (1995).
18. P. K. Rastogi, Ed., *Holographic Interferometry*, Springer Verlag, Berlin (1994).
19. R. S. Sirohi, Ed., *Speckle Metrology*, Marcel Dekker, New York (1993).
20. D. Dirksen and G. von Bally, "Holographic double-exposure interferometry in near real time with photorefractive crystals," *J. Opt. Soc. Am. B* **11**, 1858–1863 (1994).
21. M. P. Georges and P. C. Lemaire, "Phase-shifting real-time holographic interferometry that uses bismuth silicon oxide crystals," *Appl. Opt.* **34**, 7497–7506 (1995).
22. Y. Y. Cheng and J. C. Wyant, "Phase shifter calibration in phase-shifting interferometry," *Appl. Opt.* **24**, 3049–3052 (1985).
23. C. Joenathan and B. M. Khorana, "Phase-measuring fiber optic electronic speckle pattern interferometer: phase step calibration and phase drift minimization," *Opt. Eng.* **31**, 315–321 (1992).
24. C. Joenathan, "Phase measuring interferometry: new methods and error analysis," *Appl. Opt.* **33**, 4147–4155 (1994).



**S. Suja Helen** received her MSc degree in physics in 1993 from The American College, Madurai, India. Since 1995, she has been working toward her PhD degree at the Indian Institute of Technology Madras. Her research interests include phase shifting, white light interferometry, and digital image processing.



**M. H. Majles Ara** received his MSc degree in physics from Teacher Training University, Teheran, Iran, in 1986, and became a lecturer in the same university in 1987. He received his MTech in solid state technology from the Indian Institute of Technology, Madras, in 1995 under the Indo-Iranian Exchange Program. He is currently working toward his PhD in the Applied Optics Laboratory, Physics Department, IIT Madras. His current research areas include nonlinear optics, second and third harmonic generation studies in photorefractive materials and its applications in holography, image processing, and speckle metrology. He had published and presented around 20 papers in these research areas. He is a member of SPIE and the Optical Society of India.

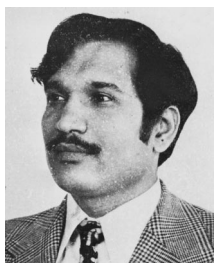


**J. S. Darlin** received his MSc degree in physics in 1990 from Kerala University, Trivandrum, and MTech degree in material technology from The Institute of Technology, Banaras Hindu University, Varanasi, in 1992. Since 1993, he has been working toward his PhD degree in the Indian Institute of Technology, Madras, where he is a senior project officer in the Applied Optics Laboratory. His research interests include optical testing and metrology, digital image processing, optical instrumentation, holography, and phase conjugation.



**N. Krishna Mohan** received his MSc (Tech) degree in applied physics from Andhra University, Waltair, and his MS and PhD degree in mechanical engineering from the Indian Institute of Technology, Madras. He worked as a visiting scientist at University Oldenburg, Germany, in 1991 under the INSA-DFG fellowship program, as a visiting scientist at Lulea University of Technology, Lulea, Sweden, in 1993 and 1995, and as an associate research officer at the National Research Council, Ottawa, Canada, in 1997. His current research areas include holographic/speckle and speckle shear interferometry, TV holography and shearography and speckle metrology using photorefractive materials. He had published and presented around 60 papers in these research areas. He is a life member of the Optical Society of India.

**M. P. Kothiyal** obtained his MTech degree in applied optics from the Indian Institute of Technology (IIT) Delhi in 1968 and his PhD degree from IIT Madras in 1977. He is currently a professor in the Physics Department at IIT Madras. He was a German Academic Exchange Service Fellow at the University of Stuttgart during 1972–74, at the University of Braunschweig during 1979–80 for three months, and at the Physikalisch Technische Bundesanstalt in 1990 for three months. He was also a research associate at Laval University, Quebec, during 1983–85. His research areas are optical instrumentation and testing, speckle methods, and polarization.



**R. S. Sirohi** received his masters in physics in 1964 from Agra University and post-MSc in applied optics and PhD in physics both from the Indian Institute of Technology New Delhi in 1965 and 1970, respectively. He was an assistant professor in the Mechanical Engineering Department at the Indian Institute of Technology Madras during 1971–1979. He has been a full professor in the Physics Department of the same institute since 1979. He worked as

Humboldt Fellow at Physikalische-Technische Bundesanstalt Braunschweig, Germany; as senior research associate at Case Western Reserve University; and as associate professor at Rose-Hulman Institute of Technology. He was a consultant from the International Center for Theoretical Physics in Trieste, Italy, to the Institute for Advanced Studies, University of Malaya. Currently he is a visiting professor at the National University of Singapore. He is a

fellow of the Optical Society of America, the Optical Society of India, and SPIE, a member of several other scientific societies, and a founding member of the India Laser Association. He was invited as a JSPS and JITA fellow to Japan. He was awarded the prestigious Humboldt Research Award in 1995 for his outstanding contributions to optical metrology. He was also chosen by the International Commission of Optics for the 1995 Galilei Galileo Award. He was president of the Optical Society of India during 1994–1996. He is on the International Advisory Board of the *Journal of Modern Optics* (UK) and on the editorial boards of the *Journal of Optics* (India) and *Optik* (Germany). He was a guest editor for the journals *Optics and Lasers in Engineering* and *Optical Engineering*. He has published 250 journal and proceedings papers and has authored/coauthored/edited 11 books. He has participated in numerous international and national conferences and presented over 100 papers. He was principal coordinator for over 20 projects sponsored by government funding agencies and industries.